



# Experimental evaluation of urban heat island mitigation potential of retro-reflective pavement in urban canyons



Federico Rossi, Beatrice Castellani\*, Andrea Presciutti, Elena Morini, Elisabetta Anderini, Mirko Filippioni, Andrea Nicolini

CIRIAF, University of Perugia, Via G. Duranti, Italy

## ARTICLE INFO

### Article history:

Received 12 January 2016

Received in revised form 13 April 2016

Accepted 14 May 2016

Available online 17 May 2016

### Keywords:

Urban heat island

Retro-reflective materials

Urban canyon

Cool pavement

Cool materials

## ABSTRACT

Retro-reflective (RR) materials have been studied as a potential mitigation technology for the Urban Heat Island (UHI) phenomenon, thanks to their ability to reflect the radiation towards the same incoming direction. In this paper, the positive effect of RR pavements on the energy kept inside the canyon was studied on a physical model that represents an urban canyon layout. The performance of RR materials was compared to that of white and beige traditional cool diffusive materials in the spectral range of the incoming radiation from 360 to 1100 nm. The objective was the evaluation of the albedo over the canyon's lid, so that also the optic interaction between pavement and façades was taken into account. In addition, the RR cooling effect, defined as the ratio between RR and diffusive reflected energies which remain inside the canyon, was calculated for the small-scale canyon scenario and the related analytical model was experimentally verified.

The results show a cooling potential of the RR material with respect to the white and the beige diffusive materials, with a maximum albedo increase of 4.6%. The cooling ratio, calculated comparing RR with the beige diffusive sample with similar global reflectance, is equal to 0.37, showing a significant decrease of the energy kept inside the urban canyon.

© 2016 Elsevier B.V. All rights reserved.

## 1. Introduction

Urban heat island (UHI) determines high temperatures in urban areas compared to the suburban ones and represents one of the most documented phenomena of climate change [1]. Dense constructions' surfaces, which absorb and store the solar radiation more than natural ones and the increase of anthropogenic heat flux are the main causes of UHI phenomenon [2]. UHI affects the energy consumptions for cooling buildings, increases the peak electricity demand during the summer period, deteriorates indoor and outdoor thermal comfort, intensifies pollution problems as the ozone concentration, increases the carbon footprint of urban facilities and utilities [3–7].

In the last years, numerous researches have been focused on the development of efficient mitigation techniques and technologies in order to counterbalance the urban overheating caused by

UHI. Cool roofs, cool pavements and urban vegetation including roof gardens and wet roofs are effective strategies able to decrease ambient and surface temperatures in cities by a few degrees [9]. A modest increase of reflectivity of urban surfaces and urban vegetation can potentially reduce the average urban temperature during the hot summer days by about 3 K [10]. Studies assess the reduction of the UHI in Athens in terms of temperature. The results offered by a MM5 climate model by comparing two modified albedo scenarios show that the temperature reduction is of 2.2 K [11]. Other studies show a temperature decrease of 1.5 K as a consequence of the albedo increase in 1250 km<sup>2</sup> of pavements in Los Angeles by 0.25. This cause also a reduction of energy consumption for cooling and reduction of pollution [12].

The effects of cool materials in terms of reduction of energy consumption, building efficiency and heat island mitigation are widely documented [13–15]. An important work about the state of art of local climate change and urban heat island mitigation techniques is developed by Akbari et al. [16]. Different types of materials are treated: white roofing materials with high solar reflectance, cool colored roofing materials, thermochromics roofing materials, directionally reflective materials, retro-reflective materials [17–25].

\* Corresponding author.

E-mail addresses: [federico.rossi@unipg.it](mailto:federico.rossi@unipg.it) (F. Rossi), [beatrice.castellani@unipg.it](mailto:beatrice.castellani@unipg.it), [castellani@ipassnet.it](mailto:castellani@ipassnet.it) (B. Castellani), [andrea.presciutti@unipg.it](mailto:andrea.presciutti@unipg.it) (A. Presciutti), [morini@crbnet.it](mailto:morini@crbnet.it) (E. Morini), [anderini.unipg@ciriaf.it](mailto:anderini.unipg@ciriaf.it) (E. Anderini), [mirko.filippioni@unipg.it](mailto:mirko.filippioni@unipg.it) (M. Filippioni), [andrea.nicolini@unipg.it](mailto:andrea.nicolini@unipg.it) (A. Nicolini).

## Nomenclature

$\alpha$	Angle between the perpendicular direction to the surface and the direction of reflection (deg, values between $-90^\circ$ and $90^\circ$ )
$\eta_0$	Reduction factor, ratio between reflector and diffusive short wave reflected energies which remains inside the canyon (adimensional)
D	Width of the urban canyon (m)
E	Irradiance ( $\text{Wm}^{-2}$ )
H	Height of the canyon (m)
n	Concentration factor (adimensional)
r	Reflectance on solar spectrum (adimensional)
$W_{r,a}$	Reflected energy in the a direction ( $\text{Wm}^{-2}\text{sr}^{-1}$ )
$W_{r,\perp}$	Reflected energy in the perpendicular direction ( $\text{Wm}^{-2}\text{sr}^{-1}$ )
$\Omega$	Solid angle (sr)
$\Omega_0$	Solid angle referred to $\alpha_0$ (sr)

Among the mentioned technologies, retro-reflective (RR) materials are an effective strategy for reducing the heat content in urban canyons and possible inter-building effects and reflecting the solar radiation beyond the urban canopy.

Studies on RR materials for building applications have been already completed by the authors [24–26]. As yet, the research was mainly focused on the analytical modelling of RR materials' behaviour for perpendicular incident radiation and the evaluation of the optic properties of RR samples for several angles of incidence.

For perpendicular radiation, the angular distribution of the reflected radiation depends on  $\cos^n$ . The exponent "n", which depends on the specific RR sample, represents a "concentration factor" of the reflected radiation around the direction of the incident radiation. A second analytical relation shows that the radiation reflected by the RR pavement which remains inside the canyon is the same of a diffusive surface but reduced by the proper factor that

depends by  $\cos^{n-1}$ . This analytical model may be used to theoretically evaluate the mitigation effects of RR materials in UHI scenarios [23].

In addition to the perpendicular direction of the incident light, the behaviour of some RR samples was also studied for different angles of incidence. Results show that RR reflect the incident radiation mainly backward to the incoming direction for low incidence angles, while for high incidence angles they reflect the radiation also symmetrically with respect to the perpendicular direction [25].

The experimental investigation in the present paper has a double objective that goes beyond the results already obtained. Firstly, the RR materials were tested as paving in a real small scale urban canyon and compared to white and beige traditional diffusive materials. The effect of the three materials on the energy kept inside the canyon and thus on the heat island phenomenon, was evaluated measuring the albedo distribution on the canyon's lid. In this way, also the optic interaction of the pavement with the surrounding façades was taken into account. Samples were previously characterized in terms of hemispherical global reflectance and reflectance angular distribution, through the following technologies respectively: (i) a spectrophotometer equipped with integrating sphere, using a flat, uniform,  $0.1 \text{ cm}^2$  sample; (ii) an ad hoc experimental facility designed on the purpose of previous research [24].

In addition, the actual RR cooling effect on real urban canyons theorized in [24] was experimentally verified and the introduced ratio between RR and diffusive reflected energies remaining inside the canyon is evaluated.

## 2. Materials and methods

### 2.1. Experimental facility

The experimental facility is located at Terni's Laboratory of Applied Physics, University of Perugia. It consists of two twin arrays, used in this paper to measure and compare the effect of reflective properties of canyon's pavement on the energy kept inside the

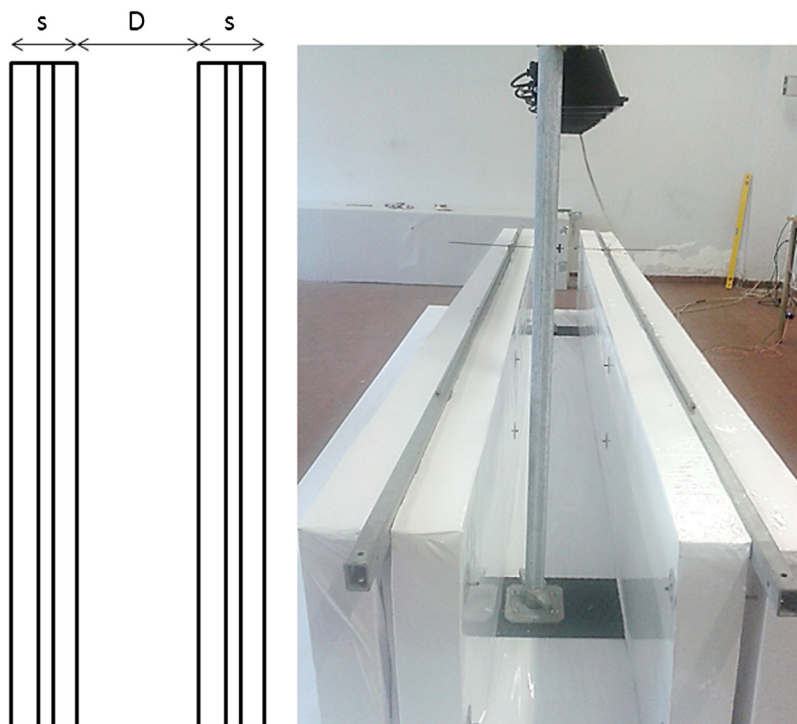
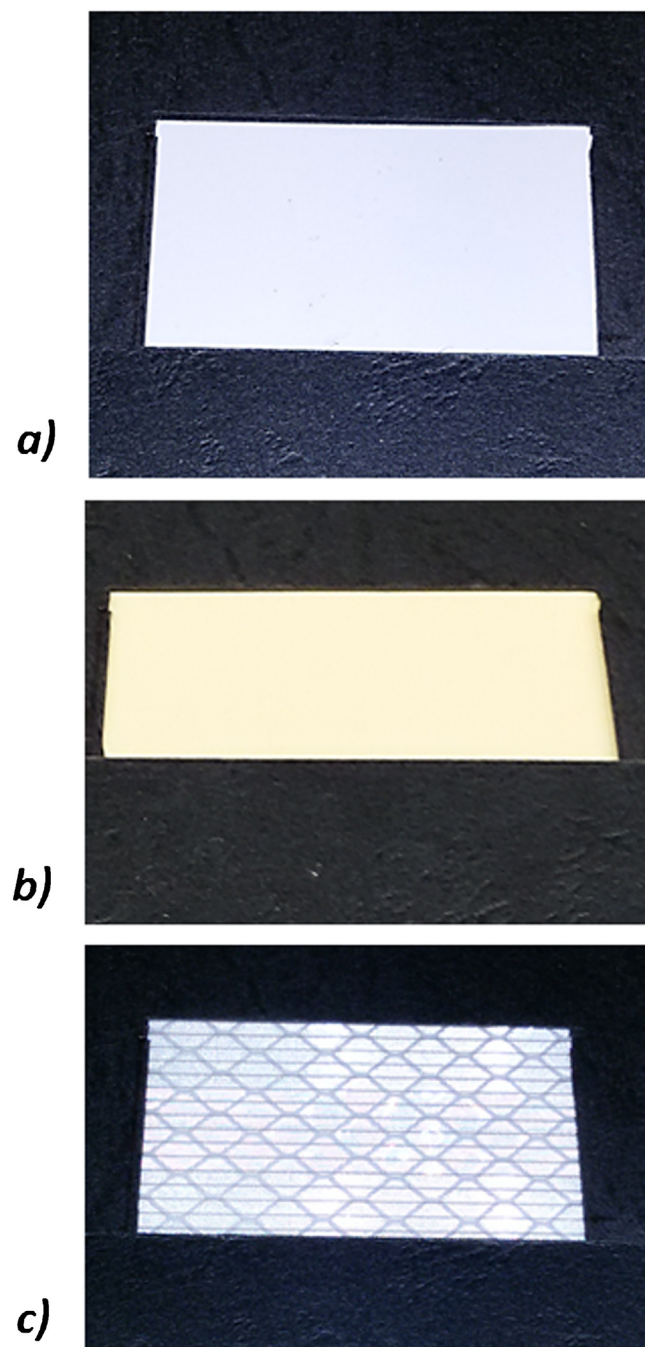
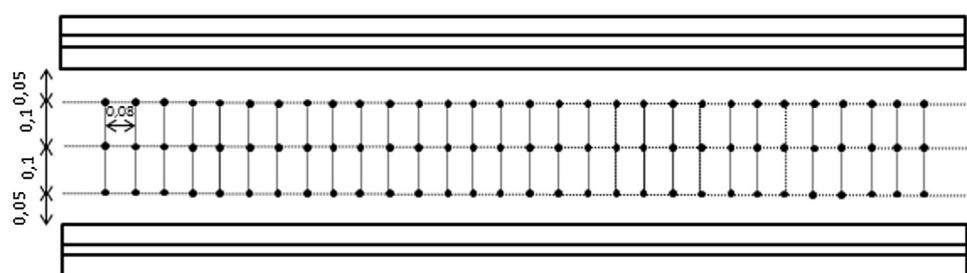


Fig. 1. Experimental facility.



**Fig. 2.** Investigated materials: (a) white diffusive (D1); (b) beige diffusive (D2) and (c) retro-reflective (RR).



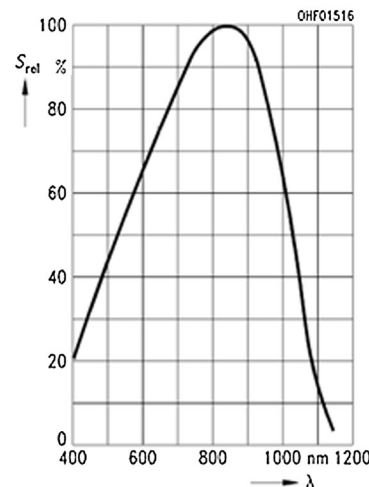
**Fig. 3.** Measurement points.

Parameter	Value	Unit
Operating and storage temperature range	-40/+100	°C
Photocurrent ( $V_R = 5$ V, standard light A, $T = 2856$ K, $E_v = 1000$ lx)	28 ( $\geq 18$ )	µA
Wavelength of max. sensitivity	860	nm
Spectral range of sensitivity	360-1100	nm
Radiant sensitive area	0,3	mm <sup>2</sup>
Half angle	±17	°
Spectral sensitivity, $\lambda = 850$ nm	0,62	A/W
Rise and fall time of the photocurrent ( $RL = 50$ Ω; $VR = 10$ V; $\lambda = 850$ nm; $I_p = 800$ µA)	10	ns
Temperature coefficient of $I_{SC}$ (standard light A, $\lambda = 950$ nm)	0,18	%/K

Relative Spectral Sensitivity

$$S_{rel} = f(\lambda)$$

SFH 229

Photocurrent  $I_p = f(E_v)$ ,  $V_R = 5$  V

$$V_O = f(E_v)$$

SFH 229

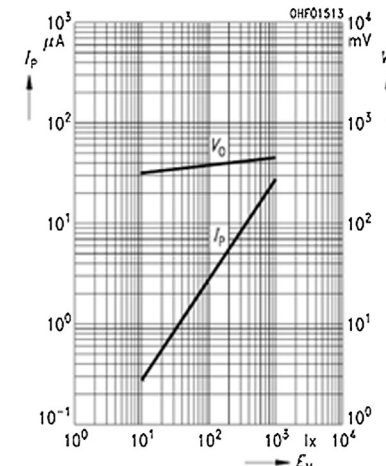


Fig. 4. Technical characteristics of SFH 229 photodiodes.

canyon. The test field is composed of two metal frames ( $H=0.6$  m and  $L=4.2$  m) supporting insulating panels ( $s=0.2$  m). The frames' distance ( $D$ ) can be modified to reproduce several canyon ratios ( $H/D$ ). In the presented configuration, the distance  $D$  was set to 0.3 m. The investigated value of the  $H/D$  ratio is 2. The canyon physical model is equipped with a lighting system to simulate the incident solar radiation. The experimental facility is shown in Fig. 1.

The vertical panels were covered with a white diffusive (D1) coating for their whole length. The horizontal surface, which represents the pavement of the canyon, was covered with three coatings characterized by different optical properties: a white diffusive film (D1), a beige diffusive film (D2) and a retro-reflective (RR) film. The used materials are shown in Fig. 2. Their optical properties are discussed in Sections 2.2 and 2.3.

The lid of the canyon is divided into an imaginary grid of 90 (3 rows  $\times$  30 columns) measurement points, at a distance of 0.08 m and 0.1 m from each other and 0.05 m from the internal edges of the canyon (Fig. 3). At each point, the reflected radiation, which goes out from the canyon, and the incident radiation, which gets in from the lighting system, are measured. The grid was used to calculate the punctual values of the albedo, given as the ratio between

the inlet and outlet radiation that cross the lid in each point, and consequently to study its variation over the surface.

The outlet reflected radiation and the incident radiation at each point is measured by an *ad-hoc* probe. The ad-hoc pyranometer was assembled using two silicon photodiodes (OSRAM SFH 229): the first one is positioned upward to measure the direct light and the second is positioned downward to measure the reflected light. The probe has a section area of  $1\text{ cm}^2$ ; thanks to the small size, the probe gives minimum disturbance during measurements. Technical characteristics of the used photodiodes are shown in Fig. 4.

The used photodiodes have a spectral sensitivity which ranges from 360 nm and 1100 nm, with a peak at 860 nm. With this sensitivity range, the photodiodes detect the visible and near IR regions, which represent nearly 70% of the solar spectrum. A black disk divides the two photodiodes and both are inserted into a black cylinder to measure only the orthogonal radiation. The outlet signal of photodiodes, proportional to the radiation, is in mV and is collected by an analog input acquisition device, supplied by National Instruments (NI 9219, NI cDAQ-9172). The ad-hoc pyranometer is shown in Fig. 5.

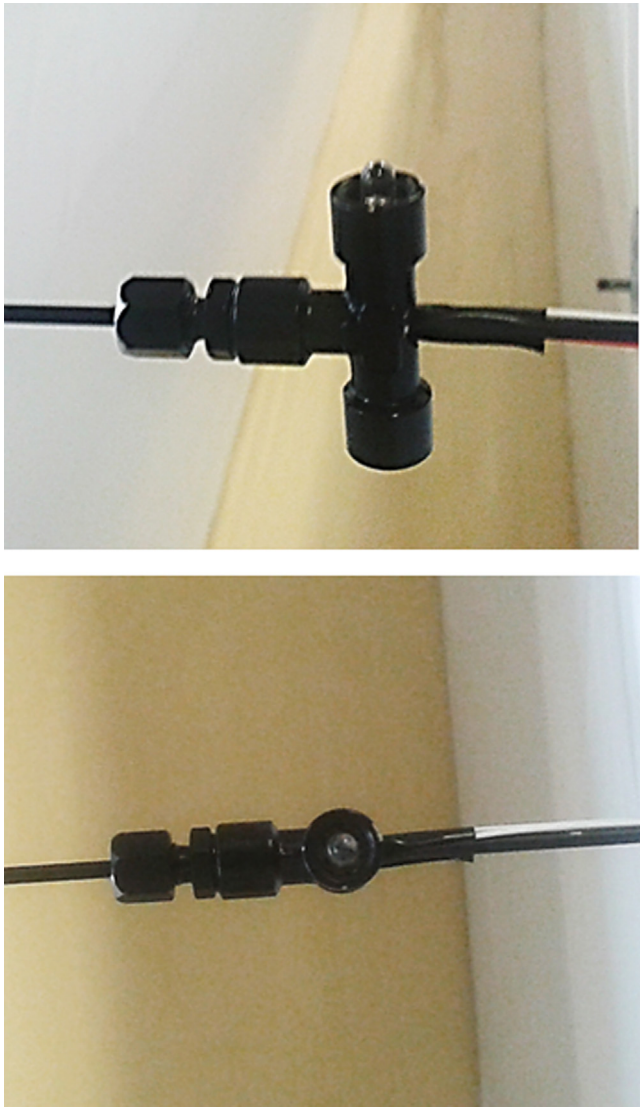


**Fig. 5.** The ad-hoc pyranometer assembled using two photodiodes.

The artificial lighting system is composed of 10 halogen lamps, supplied by Fanton SpA (model 62615), placed in the middle of the canyon at a height of 1.5 m above the ground. The power of each lamp is 1000 W, the total power is 10 kW.

The Standard IEC 60904-9 [27] was used to evaluate the spectral matching with the standard terrestrial spectrum of AM 1.5G. According to the standard, the solar spectrum from 400 to 1100 nm was divided into six intervals, and the lamps' spectrum irradiance distribution was compared to the AM 1.5 G solar spectrum distribution (Table 1). For all the wavelength ranges, the percentage of total irradiance of the halogen lamp is within the Class C solar simulators' tolerance.

Even though this standard addresses specifically solar simulators for photovoltaic applications, the considered spectral range, limited to the absorption region of silicon, fits with the responsivity and the linear range of the Si photodiodes used in the probe.

In accordance with the Standard IEC 60904-9, the spatial uniformity and temporal stability were verified.

The spatial uniformity  $U$  is calculated through Eq. (1), considering the maximum and minimum irradiance values.

$$U = \frac{E_{max} - E_{min}}{E_{max} + E_{min}} \times 100 \quad (1)$$

The lighting system's uniformity was studied using the measurement grid over the canyon's lid and is related to a spectrum range from 360 to 1100 nm. In these conditions, measurements show a non uniformity of 3.8%, less than 5% (Class B simulators, IEC 60904-9).

Long-term stability of irradiance is calculated referring to the time period of interest (the time for completing measurements on all the grid's points). The resulting irradiance variations measured in 20 min are lower than 2%. Results of these evaluations are shown in Fig. 6.

The lamps are positioned perpendicularly to the pavement in order to analyse a situation of fully illuminated pavement. The incident radiation on the ground was measured by a radiometer (HD 9221 Delta Ohm). Technical characteristics are summarized in Table 2.

The lightning system is switched on 30 min before the beginning of the acquisition phase in order to reach stationary conditions of: i) luminous flux of the lamps, ii) output signals of the photodiodes. The measured steady value of radiation on the ground is 178 W/m<sup>2</sup>. During this transient phase, also temperature on the ground is monitored continuously and its constancy is assessed before starting data acquisition. Profiles of photodiodes' output signals during the transient phase is reported in Appendix A.

For each one of the three materials tested as paving in the canyon physical model, the following experimental procedure was followed. After the transient phase, the ad-hoc pyranometer was positioned on the selected point of the measurement grid. For each point, the voltage signals from the two photodiodes are acquired ten times, every 5 s, and then averaged, obtaining  $V_{d1}$  (downward signal from photodiode 1) and  $V_{u2}$  (upward signal from photodiode 2). The same procedure was repeated after flipping the photodiodes, obtaining other two values:  $V_{d2}$  (downward signal from photodiode 2) and  $V_{u1}$  (upward signal from photodiode 1). At each point, the ratio between the downward value  $V_{d1}$ , proportional to the reflected radiation, and the upward value  $V_{u2}$ , proportional to the incident radiation, represents the albedo 1 ( $Al_1$ ) whereas the ratio between  $V_{d2}$  and  $V_{u1}$  represents the albedo 2 ( $Al_2$ ). At each point Albedo is the average value of  $Al_1$  and  $Al_2$ .

## 2.2. Spectrophotometric analysis of materials

Reflectance of the samples in the solar spectrum is measured by Shimatzu SolidSpec 3700 spectrophotometer equipped with 60 mm integrating sphere. The range of measurements is 280–2500 nm, which includes the 99% of the solar energy. The solar reflectance of the samples was then calculated using the appropriate standards (ASTM Standard G 173 [28,29]). Global hemispherical solar reflectance is equal to 86.5% for the white diffusive sample, 69.6% for the beige diffusive sample and 62.4% for the RR sample. The spectral distribution is shown in Fig. 7, where the graphs report the global reflected radiation profiles of each tested sample over the wavelength.

The three samples show similar behavior below 400 nm. In the range from 450 to 1100 nm, the white sample has the highest reflectance. At about 1300 nm the beige and the retro-reflective samples reach almost the same values and they remain very close until 2500 nm.

Hemispherical solar reflectance of the samples was calculated also in the range from 360 to 1100 nm, which corresponds to the spectral range of sensitivity of the detectors used in this work. In this range, hemispherical solar reflectance is equal to 89.7% for the white diffusive sample, 70.5% for the beige diffusive sample and 62.9% for the RR sample.

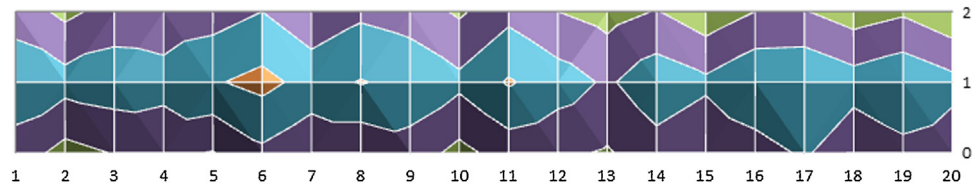
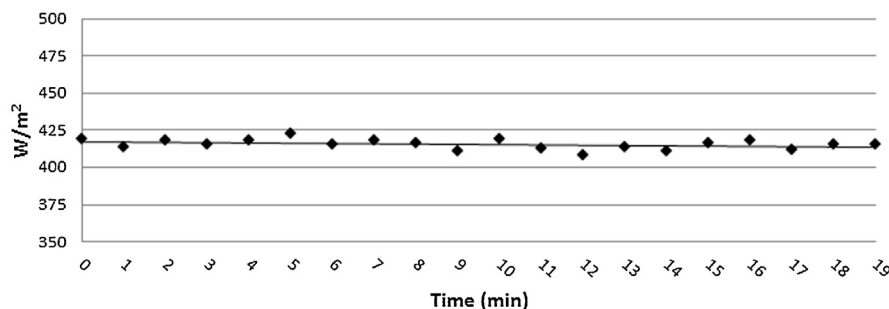
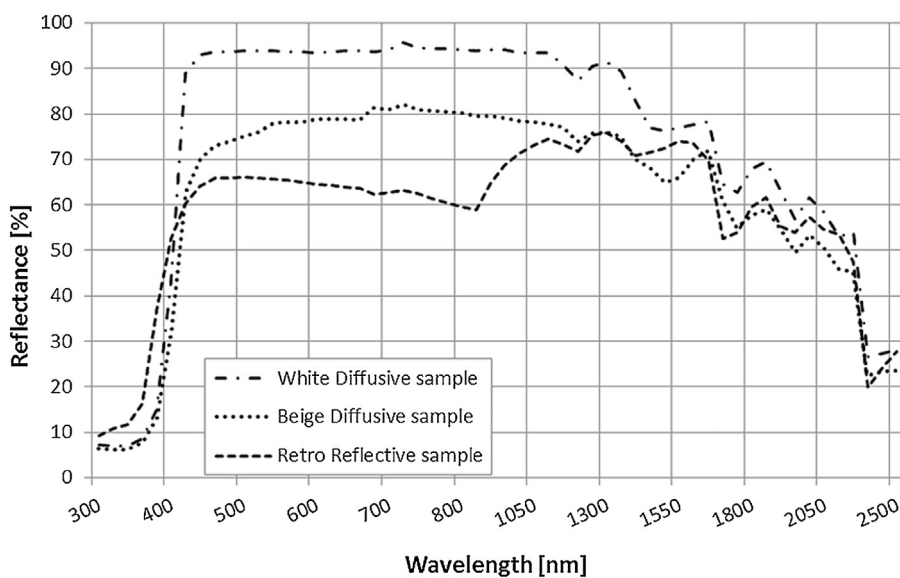
**Table 1**

Distribution of irradiance and Class C tolerances.

Wavelength (nm)	Percentage of total irradiance—AM 1.5 G	Class C tolerance (0.4–2)	Percentage of total irradiance—halogen lamp
400–500	18.4	7.3–36.8	9.5
500–600	19.9	8.0–39.8	14.1
600–700	18.4	7.3–36.8	16.7
700–800	14.9	6.0–29.8	17.0
800–900	12.5	5.0–25.0	16.1
900–1100	15.9	6.4–31.8	26.6

**Spatial uniformity - Halogen lamps**

$$\begin{aligned} E_{\min} &= 380 \text{ Wm}^{-2} \\ E_{\max} &= 410 \text{ Wm}^{-2} \end{aligned}$$

**Temporal stability - Halogen lamps****Fig. 6.** Evaluation of spatial uniformity and temporal stability of the lighting system.**Fig. 7.** Reflectance spectrum of the samples.**2.3. Angular reflectance analysis of materials**

The angular reflectance was measured through an ad-hoc experimental facility introduced in a previous study [25]. The facility was

designed and constructed in order to measure the angular distribution, i.e. directivity, of reflected radiation at several samples' tilt angles. The Si photodiodes, positioned on an arc above the samples

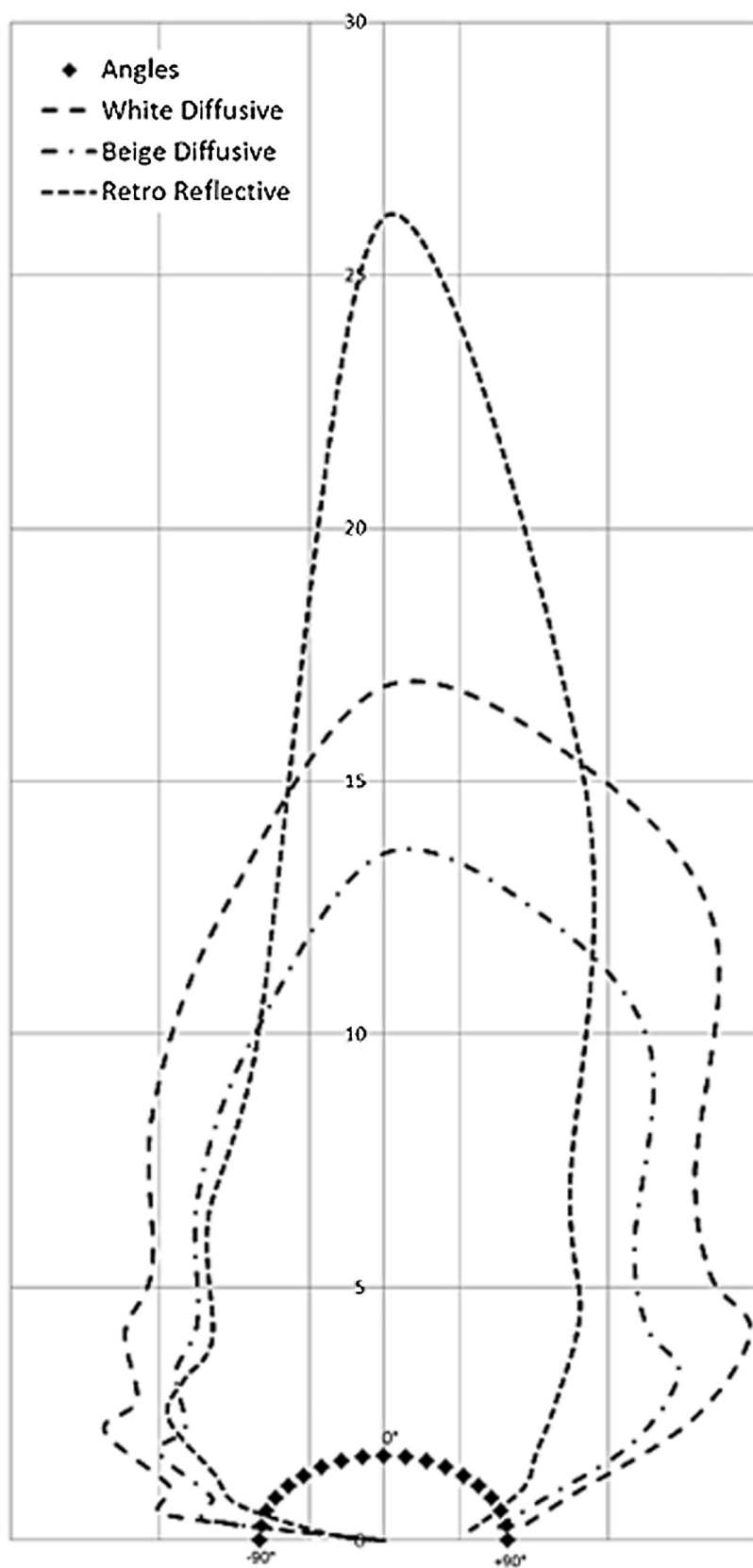


Fig. 8. Samples' angular distribution of reflected radiation.

**Table 2**

Technical characteristic of HD 9221 Delta Ohm radiometer.

Parameter	Value
Spectral range	450–950 nm
measuring range	0.1–2000 W/m <sup>2</sup>
Instrument precision	±0.15% rdg ±1 digit with a reference temperature of 25 °C ± 5 °C
Probe precision	±4%
Linearity	±1%
Stability	0.15%
Working temperature	0–50 °C

**Table 3**

Samples' angular reflectance values.

Angles	White Diffusive	Beige Diffusive	Retro Reflective
+80°	0.2	0.27	0.20
+70°	0.6	0.75	0.53
+60°	1.6	1.92	1.10
+50°	2.7	3.31	1.71
+40°	3.5	4.20	2.74
+30°	4.8	5.81	4.55
+20°	8.1	9.78	6.84
+10°	10.2	12.31	15.13
0°	11.3	13.58	26.15
-10°	8.2	9.95	9.73
-20°	5.7	6.84	6.46
-30°	3.6	4.33	3.99
-40°	2.8	3.33	3.19
-50°	1.9	2.24	2.43
-60°	1.4	1.74	1.31
-70°	0.7	0.84	0.71
-80°	0.4	0.42	0.13

every 10° from -90° to +90°, produced signal voltages proportional to the amount of reflected light in that direction. The values of the angular percentage of radiation reflected by samples for a perpendicular incident radiation are shown in Table 3 and Fig. 8.

The most of the reflected radiation by the RR sample is toward the direction of incidence. The light is reflected in an ellipse whose major axis is in the direction of the incident radiation. The diffusive samples, instead, reflect incident radiation towards all the directions, with an isotropic trend. The graph in Fig. 8 highlights the differences between the optical behavior of the RR sample compared to the optical behavior of the diffusive samples.

Indeed, the highest percentage of radiation reflected by the RR is on the 0° direction, that is the incidence direction, and it is about 26%. Instead, the percentage of radiation reflected toward the 0° direction by diffusive materials is about 17% and 14% for the white and the beige samples respectively. The peak for diffusive material is less evident and they have a more isotropic tendency.

### 3. Results and discussion

Three measurement campaigns were carried out to test different materials on the canyon pavement. On the vertical surfaces, the D1 diffusive material was always used. The first experimental campaign was carried out using the D1 material also on the ground (*White pavement case*). The second one was carried out using the D2 material on the pavement (*Beige pavement case*). The third one was carried out using the RR material on the pavement (*RR pavement case*). For each of the three cases, the amount of radiation that is reflected beyond the canyon with respect to the incident radiation is calculated over its entire superficial extension. The albedo distribution over the canyon's area is evaluated. Row 0 and 2 refer to the lateral rows; row 1 refers to the central row, in accordance with the measurement grid in Fig. 3. Results of the three experimental campaigns are shown in Table 4.

**Table 4**

Measurement results.

White diffusive pavement (D1)									
Point	Upward signal (mV)			Downward signal(mV)			Albedo ratio		
	Row 0	Row 1	Row 2	Row 0	Row 1	Row 2	Row 0	Row 1	Row 2
5	403	417	402	365	352	365	91	84	91
6	404	408	406	366	352	368	91	86	91
7	403	417	404	365	353	365	91	85	90
8	408	413	409	368	354	367	90	86	90
9	408	416	401	369	355	365	90	85	91
10	409	422	404	368	355	365	90	84	90
11	406	412	405	369	351	367	91	85	91
12	407	417	409	370	358	370	91	86	90
13	405	414	403	371	359	368	92	87	91
14	404	408	400	367	358	365	91	88	91
15	406	418	407	372	357	369	92	85	91
16	406	409	405	371	355	368	91	87	91
17	403	415	404	366	354	365	91	85	90
18	402	409	408	366	350	366	91	86	90
19	405	410	400	366	351	362	90	86	91
20	403	416	407	363	352	364	90	85	89
21	406	410	405	360	349	359	89	85	89
22	401	413	401	359	348	358	90	84	89
23	404	415	405	358	349	357	89	84	88
24	400	413	407	356	347	357	89	84	88
Beige diffusive pavement (D2)									
Point	Upward signal (mV)			Downward signal(mV)			Albedo ratio		
	Row 0	Row 1	Row 2	Row 0	Row 1	Row 2	Row 0	Row 1	Row 2
5	405	427	407	339	342	344	84	80	85
6	394	418	399	343	344	347	87	82	87
7	402	421	401	346	346	347	86	82	87
8	403	420	405	350	346	348	87	82	86
9	402	419	400	353	347	348	88	83	87
10	414	424	409	356	346	348	86	82	85
11	404	417	403	357	346	348	88	83	86
12	404	416	399	357	347	347	88	83	87
13	406	417	403	355	347	347	87	83	86
14	393	411	393	353	348	347	90	85	88
15	402	418	398	353	348	347	88	83	87
16	400	415	397	353	348	347	88	84	87
17	397	411	388	353	348	347	89	85	89
18	410	414	395	354	344	345	86	83	87
19	405	420	389	355	354	344	88	84	88
20	410	422	388	356	349	342	87	83	88
21	422	426	394	356	346	339	84	81	86
22	412	418	386	355	343	336	86	82	87
23	418	420	389	354	339	332	85	81	85
24	414	417	386	351	336	330	85	81	85
Retro reflective pavement (RR)									
Point	Upward signal (mV)			Downward signal(mV)			Albedo ratio		
	Row 0	Row 1	Row 2	Row 0	Row 1	Row 2	Row 0	Row 1	Row 2
5	406	417	406	350	357	353	86	85	87
6	397	414	398	350	358	355	88	86	89
7	401	416	404	353	358	358	88	86	88
8	402	414	404	354	362	360	88	87	89
9	400	419	406	355	365	361	89	87	89
10	408	423	410	357	368	364	88	87	89
11	402	417	403	359	366	362	89	88	90
12	402	421	408	359	366	362	89	87	89
13	406	418	406	359	364	361	89	87	89
14	397	413	399	359	363	360	90	88	90
15	405	421	407	359	366	361	89	87	89
16	402	415	400	358	364	360	89	88	90
17	399	409	396	357	360	358	89	88	90
18	406	417	401	356	363	358	88	87	89
19	402	412	394	356	362	357	89	88	91
20	406	419	400	355	363	356	88	87	89
21	412	420	401	354	363	355	86	86	89
22	402	415	395	351	360	353	87	87	89
23	407	419	399	349	360	351	86	86	88
24	405	413	392	344	355	347	85	86	88

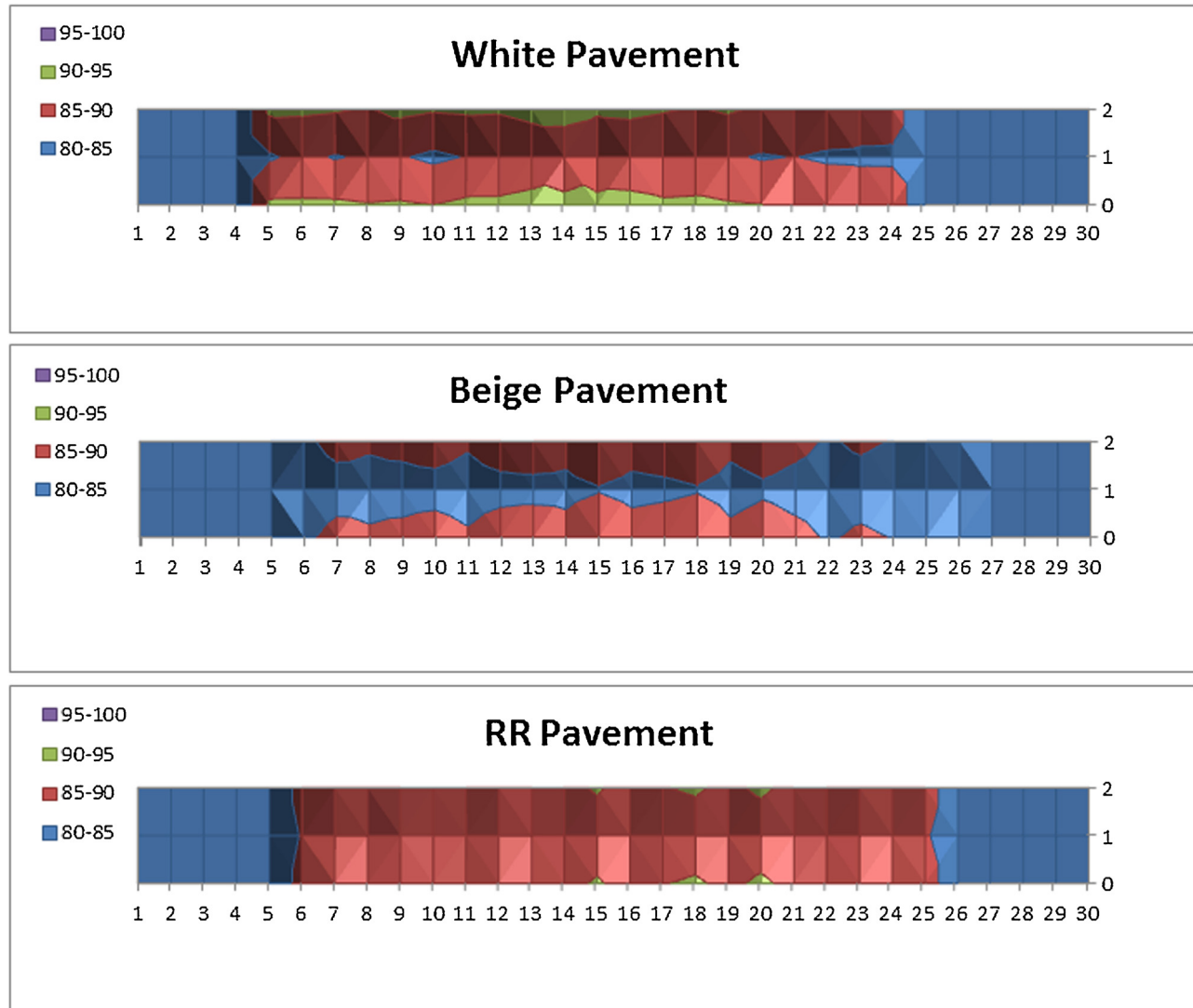


**Fig. 9.** Albedo on the canyon's upper horizontal surface for the three investigated configurations.

**Table 5**  
Average values of albedo.

Case	Row 0	Row 1	Row 2
White pavement	$90.9 \pm 0.2$	$85.7 \pm 0.2$	$90.5 \pm 0.2$
Beige pavement	$87.8 \pm 0.2$	$83.4 \pm 0.2$	$87.3 \pm 0.2$
RR pavement	$88.7 \pm 0.2$	$87.3 \pm 0.2$	$89.5 \pm 0.2$

In Fig. 9, albedo calculated in the measurement points from 5 to 24, for the three analysed configurations, are shown. The values recorded at the most external sides of the grid are not considered because they may be conditioned by edge effects.

For each row from 0 to 2, the average value of albedo was calculated and results are summarized in Table 5.

From the graphs in Fig. 9, it can be noticed that both diffusive D1 and D2 materials present the highest albedo along the external rows 0 and 2. This behaviour is particularly exacerbated for the white diffusive D1. Albedo values on the external rows are produced, not only by the direct reflection of the pavement, but also by the multiple reflections due to the interaction between pavement and façade. Considering that diffusive samples reflect only 14–17% of the light in the perpendicular direction, it follows that a significant amount of reflected radiation hits the diffusive façade, being reflected again and sent beyond the lid.

This explains the great difference between the external and central values. The albedo distribution for the RR pavement is instead quite uniform, since a higher amount of energy (26%) is sent directly backwards on the perpendicular incoming direction, reducing the extent of the successive reflection on the façades.

Comparing the average albedo in Table 5, it results that, for the reason discussed above, the D1 white diffusive material has higher values on row 0 and row 2 than the values in the D2 and RR pavement cases (the highest value is 90.9 against the 87.8 and the 88.7 respectively). Such values are also influenced by the much higher D1 overall reflectance with respect to the D2 and RR (86.5% for the D1 white material, 69.6% for the D2 beige diffusive and 62.4% for the retro-reflective sample).

However, the average value in row 1 in the white pavement case is lower than the average value in row 1 in the RR pavement case. The RR material, indeed, despite its lower value of overall reflectance, has a much higher angular reflectance towards the perpendicular (26% against the 11% and 14% of beige and white diffusive materials respectively) allowing to obtain an albedo of 87.3% against 85.7% of the D1 white diffusive.

The evaluation of the benefits of RR materials applied on canyon's pavement can be further discussed comparing the beige pavement and the RR pavement, since the global reflectance of the

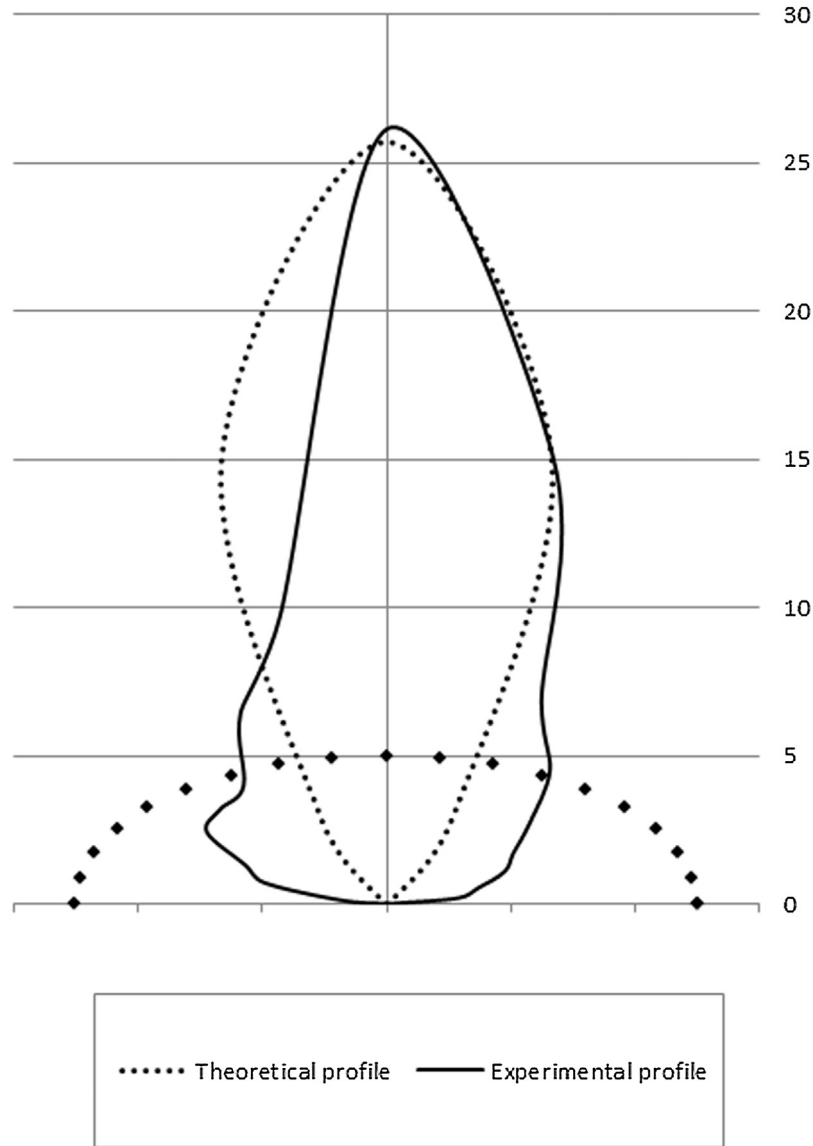


**Fig. 10.** Comparison between the experimental and theoretical profiles of RR directivities.

D2 and RR are similar. In both canyons the vertical surfaces are white (D1). The influence of D1 is the same in both canyons. The improvements are thus due to the properties of the horizontal surfaces. All the values in case 3 with RR pavement are higher than case 2 with beige pavement, both on the lateral and the central rows. The maximum increase of albedo, and therefore the percentage of radiation reflected outside the canyon, was reached in the central row and is equal to 4.6%. The near-perpendicular reflectivity, that is higher for RR than for D2, thus, mainly influences the outward radiation.

### 3.1. Experimental evaluation of the cooling potential of RR

The carried out experimental campaigns allow to demonstrate experimentally what was analytically modelled in Ref. [24]: RR surfaces contribute to reduce the energy kept inside the canyon because a part of the reflected energy is sent backward to the incoming direction outside the canyon. Considering a scenario where a perpendicular incident radiation strikes the canyon pavement made of an RR surface and comparing it with a common diffusive surface with the same hemispherical reflectance, the ratio

$\eta_0$  between RR and diffusive reflected energies, which remain inside the canyon, was calculated as:

$$\eta_0 \approx \frac{\int_{\Omega_0}^{2\pi} W_i \times r \times \frac{n+1}{2\pi} \times \cos^n(\alpha) d\Omega}{\int_{\Omega_0}^{2\pi} W_i \times r \times \frac{1}{\pi} \times \cos(\alpha) d\Omega} = \cos^{n-1}(\alpha_0) \quad (2)$$

where

$$\alpha_0 = \operatorname{atn} \left( \frac{D}{2H} \right) \quad (3)$$

with D equal to the distance between façades and H is the height of façades. The ratio  $\eta_0$ , between zero and one, represents the cooling potential of RR coatings or films when applied to an urban canyon configurations. In fact, it expresses the decrease of energy kept inside the canyon. The coefficient n, called “concentration factor”, depends on the specific RR sample and is used to calculate the distribution of the reflected radiation by a RR material in accordance with the following:

$$W_{r,\alpha} = W_{r,\perp} \cos^n \alpha \quad (4)$$

In this paper, to demonstrate the model and to calculate the cooling potential of RR in the canyon physical model with respect

to the D2 beige diffusive pavement with similar global reflectance, the following procedure is used:

- the ratio  $\eta_0$  is calculated considering experimental data on row 1. In particular, RR and D2 energies, which remain inside the canyon, are calculated as the difference between signals from upward photodiodes and downward photodiodes (see Table 4). The average value for the RR pavement is 27 mV while for the beige diffusive pavement is 73 mV, obtaining a ratio  $\eta_0$  equal to 0.37.
- $\alpha_0$  is calculated according to the canyon physical model's geometry ( $H = 0.6\text{ m}$ ,  $D = 0.3\text{ m}$ ) and is equal to 0.24.
- Knowing the ratio  $\eta_0$  and coefficient  $\alpha_0$ , it is possible to calculate the concentration factor  $n$  from Eq. (2). For the investigated RR material, it is equal to 34.
- Using Eq. (4) and considering the measured RR global reflectance equal to 0.629, the angular distribution of reflected radiation from RR materials is obtained.
- The angular distribution obtained through the application of the model is compared to the angular distribution obtained by measurement in Paragraph 2.3 Fig. 10 shows both the profiles.

For angles near to  $90^\circ/-90^\circ$ , the experimental profile deviates and gives higher values. It presents also an asymmetric tendency with respect to the normal. It is necessary to point out that real reflecting surfaces deviate from the ideal cosine laws and this is true both for diffusive materials and RR materials (See Fig. 8). Real reflection is always a composition of more than one contributions (specular, diffusive as well as retro reflection). Over the perpendicular direction, theoretical and experimental profiles match precisely.

The overlap of the two profiles confirms the validity of (Eq. (2)), providing a qualitative indication of the optic-energy behavior of RR materials and a precise evaluation of the radiation reflected beyond the canyon on the perpendicular direction.

The obtained ratio  $\eta_0$  equal to 0.37 represents the cooling potential of the RR pavement in a real small scale urban canyon, meaning a significant decrease of energy kept inside the canyon.

#### 4. Conclusions

UHI mitigation potential of RR paving was evaluated through experimental investigation on a canyon physical model, in which three different pavements were tested (white diffusive pavement, beige diffusive pavement, RR pavement), taking into account their interaction with the façades. The albedo spatial distribution over the canyon's lid was studied.

White diffusive pavements show the highest values of albedo due to the higher global reflectance. Diffusive pavements show higher values of albedo near the façades with respect to the central area of the lid. RR pavement provide instead an albedo distribution over the lid that is quite uniform. Despite its lower overall reflectance, albedo on the central area of the lid is the highest (87.3% against 86.1% of the white diffusive and 83.4% of the beige diffusive one). This is because the RR material has a higher angular reflectance towards the perpendicular (26% against the 11% and 14% of beige and white diffusive materials respectively). With respect to the beige diffusive paving with similar global reflectance, RR provides a maximum albedo increase of 4.6%. The near-perpendicular reflectivity, that is higher for RR than for the diffusive paving, mainly influences the outward radiation. The presented results were obtained through the use of sensors with a responsivity in the range of 360–1100 nm. To extend the validity of the obtained results also in the solar spectral region from 1100 nm to 3000 nm, further research with proper solar detectors is needed.

In addition, it was experimentally demonstrated that the cooling potential of RR pavements in real small scale urban canyon is actually the one theorized in previous works and proportional to  $\cos^{n-1}$ . The obtained cooling ratio  $\eta_0$  is equal to 0.37 and it indicates a significant decrease of energy kept inside the canyon physical model.

It is necessary to point out that the present investigation is a comparative analysis of the effect of the optic-energy properties of paving on the energy kept in a real small-scale physical model. At this stage of the research, other parameters that could affect the cooling potential in real scale scenarios were not taken into account. Even if RR materials have a lower global reflectance, mainly directed towards the incoming direction, i.e. upwards, further investigation is needed to evaluate glare and potential lighting pollution. Finally, future efforts will be also devoted to the production and investigation of RR materials, suitable for building applications (paintings).

#### Appendix A. Quantification of the measurement uncertainty

##### (A.1) Quantification of the measurement uncertainty

The albedo is evaluated as the ratio of the voltage output ( $V_d, V_u$ ) of two photodiodes (PD1, PD2). According to the PD technical data (Fig. 4), a resistor was used in the data logging circuit in order to obtain a linear PD voltage response to the incident radiation. Firstly, the responses of the two PDs to the same incident radiation were compared and the correlation coefficient was calculated. Results show that there is no correlation between the PDs' output signals. The average values (PD1m, PD2m) and the relative standard errors for three different values of incident radiation (related to three different values of probe's equilibrium temperature) are shown in Fig. A1. The uncertainty (random uncertainty) has to be mainly correlated to the non-stationarity of light flux of lamp.

The PDs were then placed on the canyon's lid under an incident radiation of  $350\text{ W/m}^2$  to monitor the output signal decline due to the temperature increase. As a matter of fact, PD response depends on the temperature and so signal acquisition has to begin when the PD temperature is stationary. Fig. A2 shows that the PDs under a  $350\text{ W/m}^2$  radiation reach a stationary temperature, and therefore provide a constant output signal, after 10 min.

At each point the Albedo ( $Al_1$ ) is evaluated as the ratio of  $V_d$  and  $V_u$  where the quantities  $V_d$  and  $V_u$  are the average of ten PD signal acquisitions. Then the standard uncertainty  $u(V_i)$  is calculated by the relative Type A variance. Hence the same measure ( $Al_2$ ) was carried out inverting the photodiodes, as already described in Paragraph 2.1. The final Albedo ( $Al$ ) is the average of the two ratios as shown in Eq. (A.1).

$$Al = \frac{\frac{V_{d1}}{V_{u2}} + \frac{V_{d2}}{V_{u1}}}{2} \quad (A.1)$$

According to the *Guide to the expression of uncertainty in measurement* (GUM), the standard uncertainty,  $u(Al)$ , of the calculated albedo is obtained by appropriately combining the standard uncertainties  $u(V_u)$ ,  $u(V_d)$  of the input estimates  $V_u$  and  $V_d$  and it is given by Eq. (A.2):

$$u_c(Al)^2 = \frac{\partial Al}{\partial V_1}^2 u(V_1)^2 + \frac{\partial Al}{\partial V_2}^2 u(V_2)^2 \quad (A.2)$$

where  $V_1$  and  $V_2$  values are independent or uncorrelated. Hence  $u(Al)$  is evaluated for each point. The maximum Albedo uncertainty is less than or equal to 0.2.

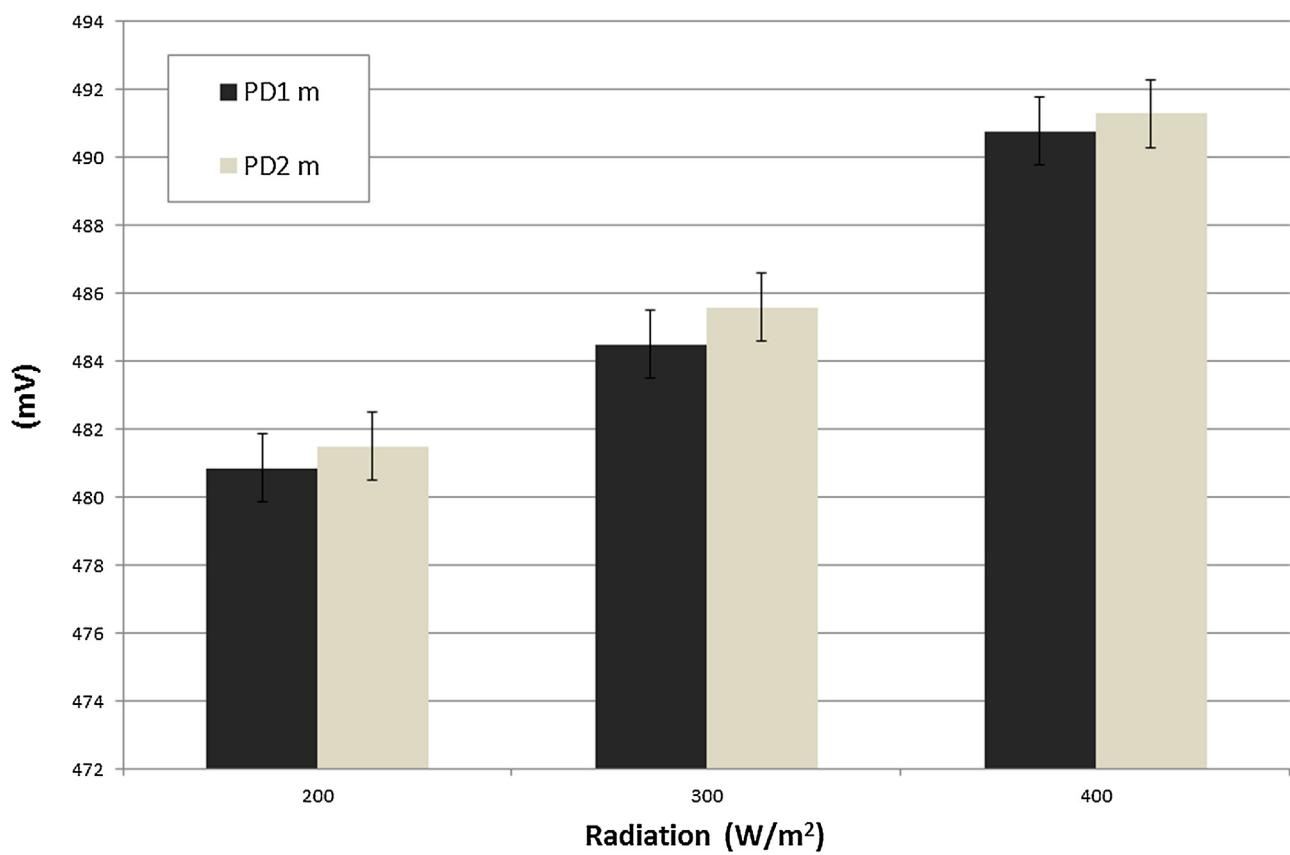


**Fig. A1.** Average values of the two photodiodes (PD1m, PD2m) and the relative standard errors for three different values of incident radiation.

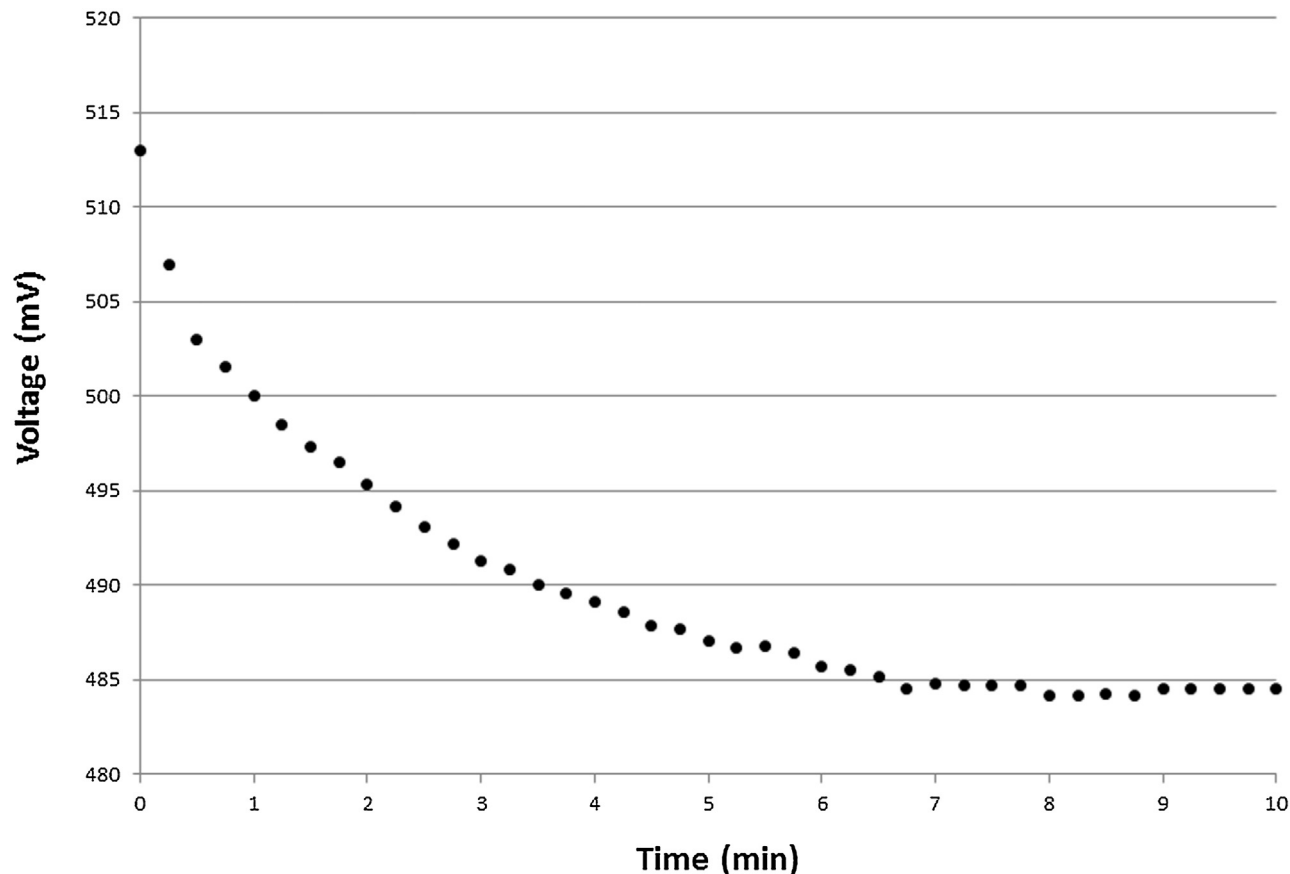


**Fig. A2.** Voltage response of the photodiodes vs time for an incident Radiation equal to 350  $\text{W}/\text{m}^2$ .

## References

- [1] M. Santamouris, *Energy and Climate in the Urban Built Environment*, James and James Science Publishers, London, 2001.
- [2] M. Santamouris, Analyzing the heat island magnitude and characteristics in one hundred Asian and Australian cities and regions, *Sci. Total Environ.* 512 (2015) 582–598.
- [3] H. Akbari, *Cooling Our Communities: A Guidebook on Tree Planting and Light Colored Surfaces*, Lawrence Berkeley National Laboratory, Heat Island Group LBNL, 1992.
- [4] M. Santamouris, Cooling the cities—a review of reflective and green roof mitigation technologies to fight heat island and improve comfort in urban environments, *Sol. Energy* 103 (2014) 682–703.
- [5] F. Rossi, E. Anderini, B. Castellani, A. Nicolini, E. Morini, Integrated improvement of occupants' comfort in urban areas during outdoor events, *Build. Environ.* 93 (2015) 285–292.
- [6] E. Stathopoulou, G. Mihalakakou, M. Santamouris, H.S. Bagiorgas, On the impact of temperature on tropospheric ozone concentration levels in urban environments, *J. Earth Syst. Sci.* 117 (2008) 227–236.
- [7] F. Rossi, E. Bonamente, A. Nicolini, E. Anderini, F. Cotana, A carbon footprint and energy consumption assessment methodology for UHI-affected lighting systems in built areas, *Energy Build.* 114 (2016) 96–103.
- [8] D. Kolokotsa, M. Santamouris, S. Zerefos, Green and cool roofs' urban heat island mitigation potential in European climates for office buildings under free floating conditions, *Sol. Energy* 95 (2013) 118–130.
- [9] H. Taha, Meso-urban meteorological and photochemical modelling of heat island mitigation, *Atmos. Environ.* 42 (2008) 8795–8809.
- [10] A. Synnefa, M. Santamouris, I. Livada, A study of the thermal performance of reflective coatings for the urban environment, *Sol. Energy* 80 (2006) 968–981.
- [11] A.H. Rosenfeld, H. Akbari, J.J. Romm, M. Pomerantz, Cool communities: strategies for heat island mitigation and smog reduction, *Energy Build.* 28 (1998) 51–62.
- [12] E. Bonamente, F. Rossi, V. Coccia, A.L. Pisello, A. Nicolini, B. Castellani, F. Cotana, M. Filippioni, E. Morini, M. Santamouris, An energy-balanced analytic model for urban heat canyons: comparison with experimental data, *Adv. Build. Energy Res.* 7 (2013), <http://dx.doi.org/10.1080/17512549.2013.865561>.
- [13] D. Kolokotsa, C. Diakaki, S. Papantoniou, A. Vlissidis, Numerical and experimental analysis of cool roofs application on a laboratory building in Iraklion, Crete Greece, *Energy Build.* 55 (2012) 85–93.
- [14] A.H. Ghaffarian Hoseini, N.D. Dahlan, U. Berardi, A.G. Hoseini, N. Makaremi, M.G. Hoseini, Sustainable energy performances of green buildings: a review of current theories, implementations and challenges, *Renew. Sustain. Energy Rev.* 25 (2013) 1–17.
- [15] H. Akbari, C. Cartalis, D. Kolokotsa, A. Muscio, A.L. Pisello, F. Rossi, M. Santamouris, A. Synnefa, H. Wong, M. Zinzi, Local climate change and urban heat island mitigation techniques—the state of the art, *J. Civil Eng. Manag.* 22 (2016) 1–16.
- [17] C. Ferrari, A. Libbra, A. Muscio, C. Siligardi, Design of ceramic tiles with high solar reflectance through the development of a functional engobe, *Ceram. Int.* 39 (2013) 9583–9590.
- [18] A. Synnefa, M. Santamouris, K. Apostolakis, On the development, optical properties and thermal performance of cool colored coatings for the urban environment, *Sol. Energy J.* 81 (2007) 488–497.
- [19] M. Zinzi, Characterisation and assessment of near infrared reflective paintings for building façade applications, in: in Proceedings of Third International Conference on Countermeasures to Urban Heat Island October 13–15, Venice, Italy, 2014.
- [20] P. Qin, J. Song, J. Qu, X. Xue, W. Zhang, Z. Song, Y. Shi, L. Jiang, J. Li, T. Zhang, The methods for creating building energy efficient cool black coatings, *Energy Build.* 84 (2014) 308–315.
- [21] T. Karlessi, M. Santamouris, K. Apostolakis, A. Synnefa, I. Livada, Development and testing of thermochromic coatings for buildings and urban structures, *Sol. Energy* 83 (2009) 538–551.
- [22] H. Akbari, A. Gholizadeh Touchaei, Modeling and labeling heterogeneous directional reflective roofing materials, *Sol. Energy Mater. Sol. Cells* 124 (2014) 192–210.
- [23] J. Yuan, C. Farnham, K. Emura, Development of a retro-reflective material as building coating and evaluation on albedo of urban canyons and building heat loads, *Energy Build.* 103 (2015) 107–117.
- [24] F. Rossi, A.L. Pisello, A. Nicolini, M. Filippioni, M. Palombo, Analysis of retro-reflective surfaces for urban heat island mitigation: a new analytical model, *Appl. Energ.* 114 (2014) 621–631.
- [25] F. Rossi, B. Castellani, A. Presciutti, E. Morini, M. Filippioni, A. Nicolini, M. Santamouris, Retroreflective façades for urban heat island mitigation: experimental investigation and energy evaluations, *Appl. Energ.* 145 (2015) 8–20.
- [26] F. Rossi, E. Morini, B. Castellani, A. Nicolini, E. Bonamente, E. Anderini, F. Cotana, Beneficial effects of retroreflective materials in urban canyons: results from seasonal monitoring campaign, *J. Phys.: Conf. Ser.* 655 (2015) 012012.
- [27] IEC 60904-9:2007. Photovoltaic devices—Part 9: Solar simulator performance requirements.
- [28] ASTM E903-12. Standard test method for solar absorptance, reflectance, and transmittance of materials using integrating spheres.
- [29] ASTM G 173-03. Standard tables for reference solar spectral irradiances: direct normal and hemispherical on tilted surface; 2012.

## Further-reading

- [8] H. Akbari, H.D. Matthews, Global cooling updates: reflective roofs and pavements, *Energy Build.* 55 (2012) 2–6.